OBSERVATIONS OF ENERGETIC HIGH MAGNETIC FIELD PULSARS WITH THE FERMI LARGE AREA TELESCOPE

D. Parent[1], M. Kerr[2], P. R. den Hartog[2], M. G. Baring[3], M. E. DeCesar[4,5], C. M. Espinoza[6], E. V. Gotthelf[7],
A. K. Harding[4], S. Johnston[11], V. M. Kaspi[14], M. Livingstone[14], R. W. Romani[2], B. W. Stappers[6], K. Watters[2],
P. Weltevrede[6], A. A. Abdo[1], M. Burgay[13], F. Camilo[7], H. A. Craig[2], P. C. C. Freire[10], F. Giordano[8,9],
L. Guillemot[10], G. Hobbs[11], M. Keith[11], M. Kramer[6,10], A. G. Lyne[6], R. N. Manchester[11], A. Noutsos[10],
A. Possenti[13], D. A. Smith[12]

ABSTRACT

We report the detection of γ-ray pulsations from the high-magnetic-field rotation-powered pulsar PSR J1119−6127 using data from the *Fermi* Large Area Telescope. The γ-ray light curve of PSR J1119−6127 shows a single, wide peak offset from the radio peak by 0.43 ± 0.02 in phase. Spectral analysis suggests a power law of index $1.0 \pm 0.3^{+0.4}_{-0.2}$ with an energy cut-off at $0.8 \pm 0.2^{+2.0}_{-0.5}$ GeV. The first uncertainty is statistical and the second is systematic. We discuss the emission models of PSR J1119−6127 and demonstrate that despite the object's high surface magnetic field—near that of magnetars—the field strength and structure in the γ-ray emitting zone are apparently similar to those of typical young pulsars. Additionally, we present upper limits on the γ-ray pulsed emission for the magnetically active PSR J1846−0258 in the supernova remnant Kesteven 75 and two other energetic high-B pulsars, PSRs J1718−3718 and J1734−3333. We explore possible explanations for the non-detection of these three objects, including peculiarities in their emission geometry.

Subject headings: gamma rays: stars — pulsars: general — pulsars: individual (PSR J1119−6127, PSR J1718−3718, PSR J1734−3333, PSR J1846−0258)

1. INTRODUCTION

Magnetic fields in neutron stars are thought to originate mainly from the fossil fields of the progenitor stars or from field generation during supernova core collapse (see, e.g., Spruit 2008). These strong fields can manifest themselves as 'classical' rotation-powered pulsars and magnetars, also known as anomalous X-ray pulsars (AXPs) and soft γ-ray repeaters (SGRs). While pulsars emit steady, beamed electromagnetic radiation from radio up to high energies ultimately via the loss of rotational kinetic energy ($\dot{E} = 4\pi^2 I\dot{P}/P^3$ erg s^{-1}), magnetars dissipate their extremely high surface magnetic fields ($B_s \sim 10^{14} - 10^{15}$ G) in luminous X-ray emission—variable on multiple time scales—generally exceeding the power derived from losing rotational kinetic energy (see Woods & Thompson 2006; Mereghetti 2008, for reviews).

The bulk of pulsar magnetic fields inferred from spin parameters are clustered around 10^{12} G. Nevertheless, a few have estimated fields near or surpassing the quantum-critical field $B_{\rm cr} = m_{\rm e}^2 c^3/e\hbar = 4.4 \times 10^{13}$ G, at which the electron cyclotron energy is equal to its rest mass. This small class of strong-field pulsars provides an opportunity to constrain emission mechanisms at high energy and to explore the interesting interface between pulsars and magnetars. Camilo et al. (2000) discovered PSR J1814−1744, the first pulsar breaking the $B_{\rm cr}$ barrier with $B_s = 5.5 \times 10^{13}$ G and $\dot{E} = 4.7 \times 10^{32}$ erg s^{-1}, and PSR J1119−6127 with a slightly weaker field. The latter object recently exhibited an unusual glitch recovery during which its radio emission shifted from its typical profile, showing an "intermittent" peak and "Rotating-Radio-Transient-like" characteristics (see McLaughlin et al. 2006, for RRATs). Weltevrede et al. (2010a) demonstrated that this type of behavior could be related to reconfigurations of the magnetic field in the magnetosphere. Moreover, PSR J1846-0258, the pulsar in the supernova remnant (SNR) Kesteven 75, exhibited the first known magnetic activity in a rotation-powered pulsar with a series of 5 SGR-like X-ray bursts and an X-ray brightening (both pulsed and DC emission) lasting about two months (Gavriil et al. 2008). A large spin-up glitch with an unusual recovery coinciding with the on-

[1] College of Science, George Mason University, Fairfax, VA 22030, resident at Naval Research Laboratory, Washington, DC 20375, USA; dmnparent@gmail.com
[2] W. W. Hansen Experimental Physics Laboratory, Kavli Institute for Particle Astrophysics and Cosmology, Department of Physics and SLAC National Accelerator Laboratory, Stanford University, Stanford, CA 94305, USA; kerrm@stanford.edu; hartog@stanford.edu
[3] Rice University, Department of Physics and Astronomy, MS-108, P. O. Box 1892, Houston, TX 77251, USA
[4] NASA Goddard Space Flight Center, Greenbelt, MD 20771, USA
[5] Department of Physics and Department of Astronomy, University of Maryland, College Park, MD 20742, USA
[6] Jodrell Bank Centre for Astrophysics, School of Physics and Astronomy, The University of Manchester, M13 9PL, UK
[7] Columbia Astrophysics Laboratory, Columbia University, New York, NY 10027, USA
[8] Dipartimento di Fisica "M. Merlin" dell'Università e del Politecnico di Bari, I-70126 Bari, Italy
[9] Istituto Nazionale di Fisica Nucleare, Sezione di Bari, 70126 Bari, Italy
[10] Max-Planck-Institut für Radioastronomie, Auf dem Hügel 69, 53121 Bonn, Germany
[11] CSIRO Astronomy and Space Science, Australia Telescope National Facility, PO Box 76, Epping NSW 1710, Australia
[12] Université Bordeaux 1, CNRS/IN2p3, Centre d'Études Nucléaires de Bordeaux Gradignan, 33175 Gradignan, France
[13] INAF - Cagliari Astronomical Observatory, I-09012 Capoterra (CA), Italy
[14] Department of Physics, McGill University, Montreal, PQ, Canada H3A 2T8

set of its magnetar-like behavior has also been reported (Kuiper & Hermsen 2009; Livingstone et al. 2010). In this context, the connection between high-B pulsars and magnetars is strengthened by the discovery of a low-B SGR which shows magnetar-like activity despite its canonical magnetic field (Rea et al. 2010).

In the high energy field for high-B pulsars, the lower energy spectral cut-off between 10 and 30 MeV observed for PSR B1509−58 in the Energetic Gamma-Ray Experiment Telescope (EGRET) era was attributed to the higher surface magnetic field (Harding et al. 1997; Thompson 2008). However, the recent discovery of GeV pulsations from the pulsar in the supernova remnant CTA1 with a comparable magnetic field and no radio counterpart showed that the emission mechanism is more complicated (Abdo et al. 2008). These observations clearly encourage closer examination of these objects to help assess if this class has unique properties from a possible overlap with magnetars.

In this paper we present γ-ray observations, acquired by the Large Area Telescope (LAT) aboard the *Fermi* Gamma-ray Space Telescope, of energetic high-B pulsars ($B \gtrsim 4 \times 10^{13}$ G) for which the spin-down energy loss rate is above 10^{33} erg s^{-1}. We report the detection of pulsed γ-ray emission from PSR J1119−6127 and discuss this detection and possible emission mechanism scenarios. We also present an upper limit on the pulsed emissions of the three other candidates including PSR J1718−3718, PSR J1734−3333, and PSR J1846−0258. Table 1 lists measured and derived parameters for the selected pulsars, ordered by their surface field strengths B_s.

PSR J1119−6127 was discovered in the Parkes multibeam pulsar survey with a period of 408 ms and a large period derivative of 4.0×10^{-12} s s^{-1} (Camilo et al. 2000). Subsequently, it was detected by XMM-*Newton* in the 0.5 - 2.0 keV range showing a single, narrow pulse aligned with the radio peak (Gonzalez et al. 2005). Besides its large surface dipole magnetic field B_s of 4.1×10^{13} G, the measurement of timing parameters infers a very young pulsar ($\tau_c = P/2\dot{P}$) of 1.6 kyr with a high spin-down power of $\dot{E} = 2.3 \times 10^{36}$ erg s^{-1}. PSR J1119−6127 is associated with the $\sim 15'$ diameter shell-type SNR G292.2−0.5 observed in both radio and X-ray bands (Crawford et al. 2001; Pivovaroff et al. 2001), as well as a compact and faint X-ray pulsar wind nebula (PWN) observed by *Chandra X-ray Observatory* (Gonzalez & Safi-Harb 2003; Safi-Harb & Kumar 2008) which is spatially coincident with the TeV source HESS J1119−614 (Djannati-Ataï et al. 2009). The SNR/PSR J1119−6127 system is located in the Galactic plane 8.4 ± 0.4 kpc away, based on neutral hydrogen absorption of X-rays from the SNR (Caswell et al. 2004). However, using the NE2001 model of the Galactic electron distribution (Cordes & Lazio 2002), we derived a distance of $16.7^{+\infty}_{-7.1}$ kpc, which places the pulsar beyond the Sagittarius arm. This discrepancy is probably due to the line-of-sight ($l = 292.151$, $b = -0.537$), which is nearly aligned with Sagittarius arm, making distance determination more uncertain than usual. In this work, we use the distance $d = 8.4$ kpc.

PSR J1718–3718 is a young pulsar with a large spin period of 3.3 s and a period derivative of $\dot{P} = 1.6 \times 10^{-12}$ s s^{-1}, implying a spin-down luminosity of $1.6 \times$ 10^{33} erg s^{-1}, the lowest of the four selected pulsars. However, it has the second highest surface magnetic field strength ($B_S = 7.4 \times 10^{13}$ G) among the known radio pulsars. It was discovered in the Parkes Multibeam Survey (Hobbs et al. 2004) not far from the direction of the Galactic Center ($l = 349.85$, $b = 0.22$), and observed as a point-like source by *Chandra X-ray Observatory* with a thermal spectrum resembling that of the transient AXP XTE J1810−197 in quiescence (Kaspi & McLaughlin 2005). Recently, deeper *Chandra X-ray Observatory* observations have shown pulsations in the soft X-ray band (0.8 - 2 keV) and better constrain the source spectrum (Zhu et al. 2011). Its distance based on a dispersion measure (DM) of 373 pc cm^{-3} is $d = 4.5 \pm 0.5$ kpc.

PSR J1734–3333 is a radio pulsar found in the Parkes Multibeam Survey (Morris et al. 2002) with $B_s = 5.2 \times 10^{13}$ G. Olausen et al. (2010) report the probable X-ray detection of the pulsar using XMM-*Newton* observations. The NE2001 model assigns a distance of $6.1^{+1.6}_{-1.0}$ kpc which, with the projected position ($l = 354.82$, $b = -0.43$), implies the pulsar is located in the Near 3 kpc Arm toward the Galactic Center.

PSR J1846–0258 was discovered in the *Rossi X-ray Timing Explorer* data (RXTE; Gotthelf et al. 2000) with $B_s = 4.9 \times 10^{13}$ G. Its spin period of 324 ms and its spin-down rate of $\dot{P} = 7.1 \times 10^{-12}$ s s^{-1} indicate this pulsar is one of the youngest known to date ($\tau_c = 723$ yr). No radio pulsed emission has been detected yet despite deep searches (Archibald et al. 2008). The distance of the associated SNR Kesteven 75 and the pulsar is still in debate. Published estimates have ranged from 6.6 kpc to 21 kpc (Caswell et al. 1975, Milne 1979, Becker & Helfand 1984). A more recent study by Leahy & Tian (2008) estimates the distance between 5.1 kpc and 7.5 kpc based on HI and ^{13}CO velocity measurements, while Su et al. (2009) in an detailed study of molecular-cloud velocities from ^{12}CO measurements determine the distance as $10.6^{+0.1}_{-1.0}$ kpc. Based on these references, we adopt in this work the distance of 7.9 ± 2.8 kpc.

2. OBSERVATIONS

2.1. *Timing Observations*

Among the pulsars considered here, three have spin-down powers above 10^{34} erg s^{-1} (see Table 1) and therefore have been followed by several observatories in the context of the pulsar timing campaign for *Fermi*, which monitors the most energetic radio and X-ray pulsars (Smith et al. 2008). This extensive program, begun in early 2007 and lasting through the *Fermi* LAT mission, provides accurate measurements of the pulsar rotation parameters used to assign phases to γ-ray photons.

PSRs J1119−6127 and J1734−3333 are observed approximately monthly with the 64-m Parkes radio telescope in Australia, at a frequency of 1.4 GHz (and occasional observations at 0.7 and 3.1 GHz). The Jodrell Bank Observatory also monitors PSR J1734−3333 on a weekly basis with the 76-m Lovell telescope, using a 64 MHz band centered at 1404 MHz connected to an analog filterbank. For these pulsars a total of 94 and 78 pulse times of arrival (TOAs) were recorded from mid-2008 to 2010, overlapping the *Fermi* LAT observations. The TEMPO2 timing package (Hobbs et al. 2006)

was used to build the timing solutions from the TOAs, which have been fitted to the pulsar rotation frequencies and their derivatives. For PSR J1119−6127, the fit includes 16 harmonically related sinusoids, using the "FIT-WAVES" option in the TEMPO2 package, to flatten the timing noise. The post-fit rms is 2.1 and 30.7 ms, or 0.5% and 2.6% of the pulsar phase, for PSRs J1119−6127 and J1734−3333 respectively. Full details of the observing and data analysis can be found in Weltevrede et al. (2010b) and Hobbs et al. (2004).

PSR J1718−3718, due to its relatively low spin-down power, is not a target for the *Fermi* campaign. We used a timing solution constructed as outlined in Manchester & Hobbs (2010). Timing observations were made between 2009 January 24 and 2009 June 19 using the Parkes radio telescope with the 10-cm receiver, which has a 1024-MHz bandwidth centered at 3100 MHz, and the Parkes digital filterbank system. The resulting timing solution based on 23 TOAs has a post-fit rms of 3.4 ms.

Finally, X-ray timing observations for PSR J1846–0258 were made weekly using the Proportional Counter Array (PCA; Jahoda et al. 1996) on *RXTE*, and were collected in "Good Xenon" mode. Photons arriving between 2008 June 5 and 2010 April 6 were extracted from the first xenon detection layer in the energy range 2 - 20 keV, and folded with the previously published ephemeris (Livingstone et al. 2010). The resulting pulse profiles were cross-correlated with a high significance template, producing a single TOA for each observation. The TOAs were fitted to a timing model using the pulsar timing software package TEMPO[15]. Further details of the analysis can be found in Livingstone et al. (2006) and Livingstone et al. (2010). Note that the detailed description of the timing analysis and results for PSR J1119−6127 using the PCA instrument are given in §3.3.

The timing parameters used in this work will be made available from the *Fermi* Science Support Center[16].

2.2. *Gamma-ray Observations*

The LAT aboard *Fermi* is an electron-positron pair conversion telescope and went into orbit on 2008 June 11 (Atwood et al. 2009; Abdo et al. 2009). The telescope covers the 20 MeV to > 300 GeV energy range with good sensitivity and localization performance (an effective area $\sim 8000\,\mathrm{cm}^2$ on-axis above 1 GeV and an angular resolution $\theta_{68} \sim 0.6°$ at 1 GeV for events in the front section of the tracker). The LAT timing is derived from a GPS clock on the spacecraft, and γ-rays are hardware time-stamped to an accuracy significantly better than $1\,\mu s$ (Abdo et al. 2009).

3. ANALYSIS AND RESULTS

3.1. *Data Selection*

For each pulsar, we selected LAT data collected between 2008 August 4 (MJD 54682) when *Fermi* began scanning-mode operations[17] and the end of the ephemeris

---

[15] http://www.atnf.csiro.au/research/pulsar/tempo
[16] http://fermi.gsfc.nasa.gov/ssc/data/access/lat/ephems
[17] Except for J1718–3718 for which the timing solution starts at 54855 MJD.

validity range (17–29 months). We used "diffuse" class events (highest probability of being γ-ray photons) under the P6_V3 instrument response function (IRFs), and excluded events with zenith angles > 100° to reject atmospheric γ-rays from the Earth's limb. In addition, we also have excluded for the spectral analysis time intervals when the region of interest (ROI) intersects the Earth's limb. The events were analyzed using the standard software package *Science Tools-09-21-00*[18] (ST) for the *Fermi* LAT data analysis and photon phases were calculated using the "*Fermi*-plugin" available in the TEMPO2 pulsar timing software (Ray et al. 2011).

Multiple scattering at low photon energy dominates the LAT's angular resolution. To approximate as much as possible the instrument *Point Spread Function* (PSF), we selected events for the light curves with an energy-dependent angular radius cut centered on the studied pulsar. This selection is given by $< \theta_{68}(E) > = [(5.12°)^2 \times (100\,\mathrm{MeV}/E)^{1.6} + (0.07°)^2]^{1/2}$ which approximates a 68% containment angle according to the IRFs.

We searched for γ-ray pulsations using the bin-independent H-test (de Jager & Büsching 2010), and selecting photons passing the energy-dependent cut for different maximum angular radii (from 0.5 to 5 degrees) around the pulsar position and energy bands. This truncates the point-spread function at low energies and decreases the number of background events. After taking the number of trials into account, we detected a pulsed γ-ray signal from PSR J1119−6127 with a significance above $5\,\sigma$ (our detection threshold). For the other pulsars we found significances below $3\,\sigma$ as discussed in § 3.5.

3.2. *Gamma-ray Study of PSR J1119−6127*
3.2.1. *Light Curves*

Figure 1 presents the 20 bin γ-ray phase histograms in three energy ranges, along with the radio profile and the X-ray profile observed by XMM-*Newton* (bottom panels). The top panel shows the profile with optimized signal-to-noise ratio, corresponding to an event selection above 0.5 GeV within 0.5 of the timing position and passing the energy-dependent cut. For this energy band, the H-test gives a value of 107 corresponding to a pulsation significance of $9\,\sigma$. The dashed line shows the background level (76 counts per bin) estimated using an annular ring centered on the radio position, during the off-pulse window ($\phi < 0.10$ and $\phi > 0.65$), and with inner and outer radii of 0.5 and 1.5, respectively. No significant pulsed signal was detected below 0.5 GeV, despite searches using different apertures. The light curve consists of one single, wide peak observed between 0.10 and 0.65 in phase, which defines our on-pulse window. The light curves between $0.5-1$ GeV and above 1 GeV within the same aperture have similar pulse profiles. We fitted the unbinned γ-ray data above 0.5 GeV with a Gaussian function. The peak is offset in phase from the radio peak by $\delta = 0.43 \pm 0.02$ with a FWHM of 0.18 ± 0.03. The bias due to the DM uncertainty in extrapolating the radio TOA to infinite frequency is negligible.

3.2.2. *Spectrum*

---

[18] http://fermi.gsfc.nasa.gov/ssc/data/analysis/scitools/overview.html
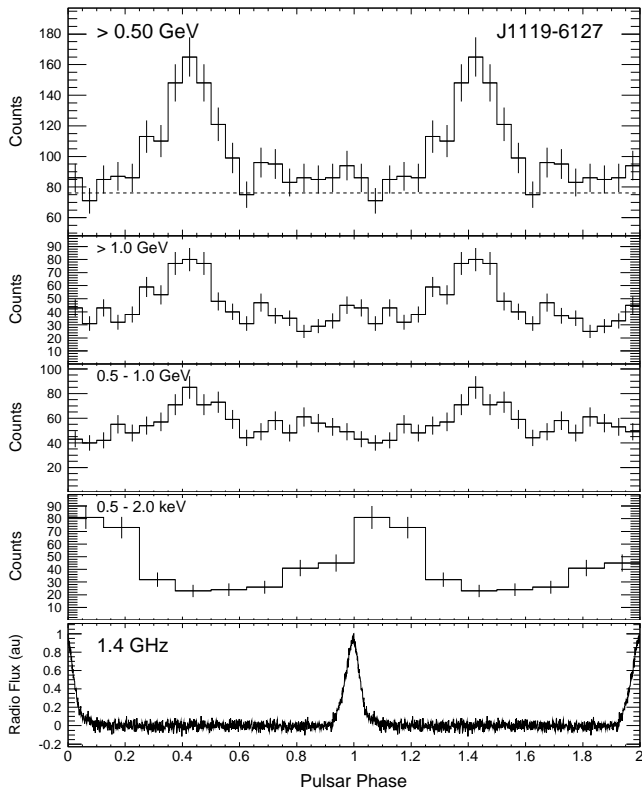
FIG. 1.— Phase-aligned radio, X-ray, and γ-ray profiles of PSR J1119−6127. Bottom panel: 1.4 GHz radio profile observed with the Parkes telescope. Second panel from bottom: X-ray profile in the 0.5–2.0 keV ranges observed by *XMM* (adapted from Gonzalez et al. 2005). Top panels: γ-ray profiles obtained with the *Fermi* Large Area Telescope in different energy bands. Two rotations are shown. The dashed line shows the background level estimated from a surrounding ring.

A phase-averaged spectrum was obtained with a binned likelihood analysis (Mattox et al. 1996) of the LAT data selected from $20° \times 20°$ region centered on the pulsar position, using the *Fermi* Science Tool "gt-like". The Galactic diffuse emission was modeled using the *gll_iem_v02* map cube, while the extragalactic emission and residual instrument backgrounds were modeled jointly by the isotropic component *isotropic_iem_v02*. These two models and an explanation of their development are available from the FSSC. In addition, all point sources within $15°$ of the pulsar found in an updated version of the LAT 1FGL source catalog (Abdo et al. 2010b), using 18 months of data, were included in the model. Sources were modeled with a power law spectrum, except for pulsars, for which a power law with an exponential cut-off was used (see Eq.1 and Abdo et al. 2010d). Sources more than $5°$ from the pulsar were assigned fixed spectra taken from the source catalog. Spectral parameters for sources within $5°$ of the pulsar were left free for the analysis. We fitted the spectrum of PSR J1119−6127 above 100 MeV using an exponentially cut-off power-law of the form

$$\frac{dN}{dE} = N_0 E^{-\Gamma} \exp\left[-\left(\frac{E}{E_c}\right)^\beta\right] \text{cm}^{-2}\,\text{s}^{-1}\,\text{MeV}^{-1}, \quad (1)$$

where N_0 is the differential flux (in units of $\text{ph cm}^{-2}\,\text{s}^{-1}\,\text{MeV}^{-1}$), Γ the photon index, and E_c the cut-off energy. The parameter β, which determines the steepness of the exponential cut-off, was fixed to 1. The *Fermi* LAT pulsars are generally well-described by a simple exponential model, $\beta = 1$, a shape predicted by outer magnetosphere emission models (Abdo et al. 2010d). The energy at which the normalization factor N_0 is defined is 1 GeV. The best-fit values are listed in Table 1 as well as both the photon flux F_{100} and energy flux G_{100} above 100 MeV, where the first errors are statistical and the second are systematic. The systematic uncertainties were estimated by applying the same fitting procedures described above and comparing results using bracketing IRFs where the effective area has been perturbed by $\pm$ 10% at 0.1 GeV, $\pm$ 5% near 0.5 GeV, and $\pm$ 20% at 10 GeV with linear interpolations in the logarithm of the energy for intermediate energies. We also modeled the pulsar with a simple power-law spectrum ($\beta = 0$), and by leaving the β parameter free in Equation 1. In the first case, the exponentially cut-off power law model is preferred at the $6\,\sigma$ level according to the likelihood ratio test (Mattox et al. 1996), while in the second case the extra free parameter did not improve the quality of the fit. The results were all cross-checked using an alternate analysis tool developed by the LAT team. Figure 2 shows both the phase-averaged spectral fit between 0.1 and 10 GeV (solid lines) with $\beta = 1$, and the spectral points derived from likelihood fits to each individual energy band in which it was assumed the pulsar had a power-law spectrum.

To search for unpulsed emission from a compact nebula or magnetospheric emission from the pulsar, we searched in the off-pulse region ($\phi < 0.10$ and $\phi > 0.65$) for a point source in the energy band $0.1 - 100$ GeV at the radio pulsar position. Using a power-law spectrum we found a $7\,\sigma$ signal with an energy flux above 0.1 GeV of $(2.0 \pm 0.3) \times 10^{-11}$ erg s^{-1} which represents $\sim$ 30% of the phase-averaged emission. There are three possibilities to explain this signal: emission from a PWN or SNR, magnetospheric pulsar emission, or unmodeled structure in the Galactic diffuse emission. To determine its origin, we fitted the signal in three energy bands (0.1 - 1 GeV, 1 - 10 GeV, 10 - 100 GeV) and in the whole energy range (0.1 - 100 GeV) using a pulsar shape spectrum (see eq. 1). The signal is only significant below 1 GeV and the exponentially cut-off power law model is preferred over a simple power-law model at the $5\,\sigma$ level, with a spectral index of 0.2 ± 1.0 and an energy cut-off of 0.3 ± 0.2 GeV. An exponentially cut-off spectrum, which has been observed in the off-pulse of a few pulsars (Ackermann et al. 2011), suggests a magnetospheric origin. However, the model for the Galactic diffuse emission is imprecise in this complex region, and such features may also be associated with unmodeled structure in the Galactic diffuse emission. In particular, the apparent low energy cut-off may be a result of the large PSF at low energies ($\theta_{68} \sim 3°$ at 100 MeV for events in the front section of the tracker). If the emission is in fact an inadequately-modeled diffuse component, the phase-averaged γ-ray flux for PSR J1119−6127 would be reduced by 30%. However, because the emission is only present in a narrow band at low energy, we expect

the phase-averaged spectral shape to remain largely unchanged.

Finally, the pulsar associated to the source 1FGL J1119.4−6127c does not show any variability in the 1FGL catalog and an internal 18-month LAT source list (Abdo et al. 2010b). But in view of the recent evidence for changes in the magnetospheric configuration of PSR J1119−6127, a careful search for changes in the spectrum and pulse shape is warranted if a glitch occurs.
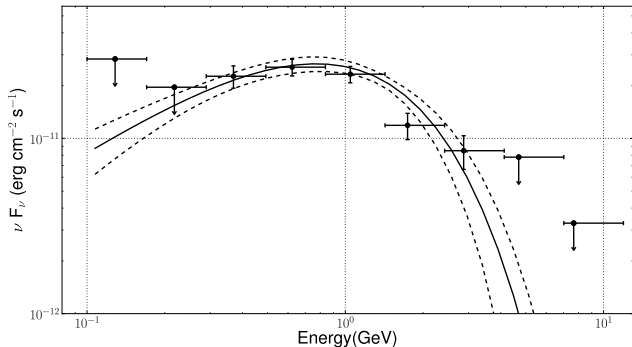

FIG. 2.— Phase-averaged spectral energy distribution of PSR J1119−6127 in γ-rays obtained with the *Fermi* Large Area Telescope. Plotted points are from likelihood fits to individual energy bands with $\geq 4\,\sigma$ detection above background for two degrees of freedom, otherwise an upper limit arrow is shown. The solid black line shows the maximum likelihood fit to a power law with exponential cut-off (Eq. 1). The dashed lines are $\pm\,1\,\sigma$ uncertainties on the fit parameters.

3.3. *X-ray Study of PSR J1119−6127*

We also searched for pulsed X-ray emission from PSR J1119−6127 to compare to our *Fermi* results. The pulsar was monitored regularly as part of an *RXTE* monitoring campaign[19] to look for magnetar-like behavior as discovered from PSR J1846−0258 (Gavriil et al. 2008). Data were collected using the PCA, an array of five collimated xenon/methane multi-anode proportional counter units (PCUs) sensitive to incoming photons in the 2 - 60 keV energy range, with a total effective area of approximately 6500 cm^2 and a field of view of $\sim 1°$ FWHM. We used all archival XTE data available in HEASARC public archive[20] on the pulsar that spanned the valid interval time of the radio ephemeris. All data were taken in high time resolution Good-Xenon mode ($>100\,\mu s$). These data sets were processed using the standard reduction and analysis tools. After extracting time intervals contaminated with PCA breakdown events, the data were merged into a single barycenter corrected FITS photon file. We selected counts from the first layer and energy range up to 20 keV and folded the data with the same ephemeris used to analyze the *Fermi* LAT data (see §3.1). No significant signal was found in the XTE data range (MJD 54890 - 55170). This is not surprising since the X-ray pulsed emission detected by Gonzalez et al. (2005) shows strong energy dependence and appears to be confined to the soft X-ray band below 2 keV. We then folded

[19] PI: F. P. Gavriil
[20] http://heasarc.gsfc.nasa.gov/docs/archive.html

data from energy bands restricted to the lowest energy PI channels to test all cumulative channels up to 5 keV. However, again no signal was detected.

3.4. *Emission Models of PSR J1119−6127*

The first year of pulsar studies with *Fermi* has shown that the γ-ray emission mechanism for young pulsars is likely to be outer magnetospheric in origin (Abdo et al. 2010d). Such emission is predicted by several different models. The Outer Gap models (OG, Cheng et al. 1986a,b; Romani 1996) place the emitting region on a set of open zone field lines paralleling the closed zone boundary; particles accelerate and radiate between the 'null charge' surface and the light cylinder, so that only one magnetic pole is visible in each hemisphere and the hollow cone produces the typical double γ-ray pulse. An alternative picture is the two-pole caustic model (TPC, Dyks & Rudak 2003) which uses a similar set of field lines, but posits acceleration starting near the star surface; both poles are visible in both hemispheres and a double pulse is formed by truncating the emission zone at $\sim 0.8\,r_{LC}$ so that only the trailing edges of the two cones are present in the light curve. More physical pictures, e.g. the slot-gap model (SG, Muslimov & Harding 2004), may have radiation from a wide range of altitudes and so may be approximated by either of these two geometries.

We can compare the predictions of the OG and TPC pictures following the procedure in Romani & Watters (2010). For these calculations we assume a co-rotating vacuum-like field ('pseudo-force-free'), model the field for a gap width $w = (10^{33}\mathrm{erg\,s}^{-1}/\dot{E})^{1/2}$ of 0.02 for PSR J1119−6127, and compute the light curve for each magnetic inclination angle α and viewing angle ζ. In Figure 3 we compare the match between the model light curve and the data in the (α, ζ) plane using the χ_3 weighting defined in Romani & Watters (2010); dark colors are better fits. For PSR J1119−6127, as for many young *Fermi* pulsars, the radio emission has high linear polarization and has been fit to the rotating vector model (RVM) to constrain the geometrical angles α and ζ (e.g., Crawford & Keim 2003). Even better constraints can be obtained from the unusual double-peaked mode found by Weltevrede et al. (2010a) in post-glitch timing observations. We fit the RVM model to these data and correct for the RVM sign convention problem (Everett & Weisberg 2001) to obtain the allowed range (green contours) in Figure 3. As is often the case, these fits primarily constrain $\beta = \zeta - \alpha$; the 0.5, 1.5 and 2.5 σ contours from these fits are shown.

The idealized RVM model assumes a point dipole and does not account for the radio emission altitude or the magnetosphere closed zone. If the radio emission arises from finite altitude, the phase and shape of the pulse maximum and the radio polarization sweep are shifted (Blaskiewicz et al. 1991; Dyks & Harding 2004). We have used our numerical models of the magnetospheric field structure to fit the polarization sweep for finite altitude radio emission, requiring that the observed radio flux arise from open field lines. The best fits are found for altitudes $\approx 0.1\,r_{LC}$; we show the contours of the allowed regions in the left (OG) panel of Figure 3. While the allowed α, ζ range is quite similar to that of the
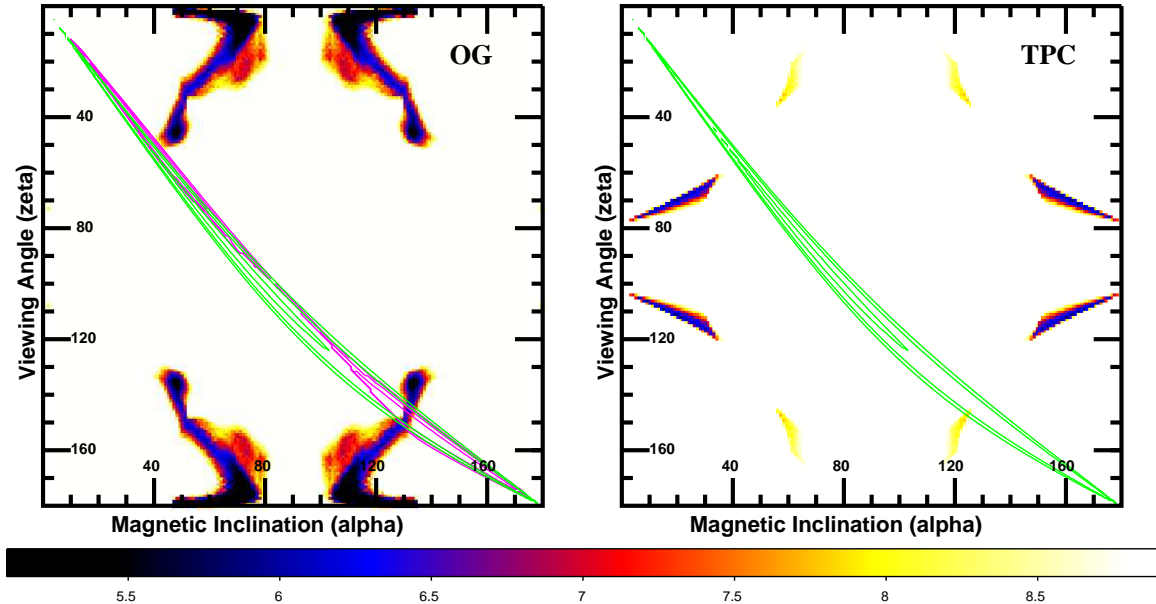
FIG. 3.— Pulsar geometry and emission modeling for PSR J1119−6127 for the 'Outer Gap' (left panel) and the 'Two Pole Caustic' (right panel) models in the magnetic inclination − viewing angle (α, ζ) plane. Green contours show the RVM fit to the Weltevrede et al. (2010a) radio polarization data. For the left panel we also show the polarization fit for finite altitude, open zone radio emission ($r = 0.09\,r_{LC}$, magenta contours). Contours are at $1.5\times$, $2.5\times$, and $3.5\times$ the minimum value of the reduced $\chi^2 = 0.85$. The background color scale gives the χ_3 statistic fit to the observed $> 500\,\mathrm{MeV}$ pulse profile. The color scales in the panels are the same, with dark colors representing better fits. Preferred models lie along the diagonal polarization fit band.

RVM fit, the phase constraints provide important additional information. In Figure 4 we show the observed and model light curves for the radio emission for α and ζ at the best values allowed by the γ-ray pulse shape and polarization constraints in Figure 3. The lower panel shows the Parkes radio light curve in the double-peaked mode. The corresponding positional angle (PA) sweep of the polarization vector is shown in the upper panel (right scale). The phasing is set by the fit (green dotted line) to the maximum rate of the PA sweep, $\mathrm{d}\Psi/\mathrm{d}\phi_{\max}$ (top panel). This fit is very good for the inferred angles ($\chi^2/\mathrm{DoF}=1.1$) and, in turn, determines the phase of the closest approach of the surface magnetic dipole axis to the Earth line-of-sight. This is denoted by the pulsar phase $\phi_B = 0$. Note that the phase of the observed pulse centroid ($I_{\max}$, lower panel) is offset from the dipole axis. The intensity and PA offsets are in the same sense as the analytic approximation by Blaskiewicz et al. (1991), but field line sweep back distortion (Dyks & Harding 2004) makes the offsets smaller, implying a higher emission altitude. Note also that Weltevrede et al. (2010a), using the Blaskiewicz et al. (1991) approximations, derived a lower emission height. Thus to fit the observed pulse width into the open zone they argued for small α. With the numerical modeling of the polarization sweep and pulse offset we derive larger heights and find that the observed sweep and pulse profile are well matched for angles consistent with the γ-ray data, while having the radio emission arise from the open zone.

We can now compare with the observed *Fermi* γ-ray light curve (Figure 4, upper panel). Adding the constraints supplied by the polarization data restricts the acceptable region. For the OG model the best γ-ray fits consistent with the polarization constraints are at

$\alpha = 125 - 130°$, $\zeta = 140 - 150°$. For the TPC picture best fits in the allowed range are also near $\alpha = 125°$, $\zeta = 145°$, however this model gives a poorer pulse profile ($\chi_3 = 8.1$ v.s 6.0) fit than the OG case (Figure 3). The *Fermi* light curve is referenced to the radio pulse peak (in the single-peaked mode) and the observed radio-peak/γ-pulse offset is $\delta = 0.43$. The γ-ray pulse models are computed relative to the magnetic axis ($\phi_B = 0$); we find that the best-fit OG light curve (solid line), in fact, has phase $\phi_B = 0.39$ for altitudes of $\approx 0.1\,r_{LC}$, corresponding to $\delta = 0.43$. The model pulse is single, with little off-pulse emission. Using the phase and viewing angles determined by the radio observations, the best-fit TPC model has two peaks and a large unpulsed component (Figure 4). For these models the flux correction factors are $f_\Omega = 1.50$ (OG) and $f_\Omega = 0.95$ (TPC).

Note that these fits assume the background level inferred from the surrounding ring. If, in contrast, the true minimum of the magnetospheric flux is the baseline level at $\phi = 0.65 - 0.1$, then we find that the OG light curves fit much better than the TPC case ($\chi_3 = 2.0$ vs. 11.3); the best fit α and ζ are nearly unchanged.

We conclude that, in the context of these simple geometrical models, the high altitude component conventionally associated with the OG model is the preferred origin of the observed γ-ray pulse, with an excellent match to the observed pulse phase and light curve shape. However, as for other single-peaked γ-ray pulsars it is difficult to exclude other model scenarios. In particular, some versions of the slot gap models that allow emission at larger altitudes may provide a good fit to the light curve; we will need higher sensitivity to search for the fainter low altitude off-pulse emission predicted to occur in these models. Also, more physical realizations of
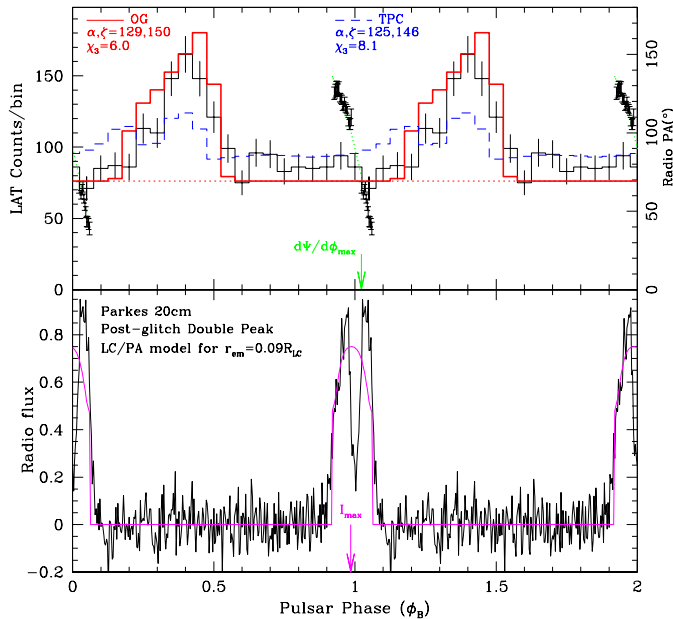
FIG. 4.— Light curves for PSR J1119−6127. The bottom panel shows the Parkes radio light curve in the two peaked (post-glitch) mode, which provides the best model constraints. The corresponding radio polarization position angle data are shown (right scale) in the upper panel. The model Pulsar Phase (ϕ_B) is referenced to the closest approach of the magnetic axis to the Earth line-of-sight, as fit from the polarization sweep. The sweep rate maximum (green arrow) and pulse profile offsets (magenta arrow) are shown, with good matches to the observed radio data for an altitude of $r = 0.09\,r_{LC}$. The upper panel shows the LAT pulse profile (left scale) and model OG (solid line) and TPC (dashed line) profiles. These are best-fit profiles (geometric angles in the legend) and the phase is referenced to the radio-determined phase of the magnetic axis. The γ-ray background, shown by the dotted line, was estimated using an annular ring centered on the radio position with inner and outer radii of $0.5°$ and $1.5°$ respectively, during the off-pulse region.

the pulsar magnetosphere, such as the numerical force-free 'Separatrix Layer' (SL) model of Bai & Spitkovsky (2010) may produce acceptable light curve fits. In summary, we find that the light curve of J1119−6127 can be well fit by conventional γ-ray pulsar models but only when emission from relatively close to the light cylinder dominates. Despite the object's high surface magnetic field, the field strength and structure in the γ-ray emitting zone are apparently similar to those of more typical young pulsars.

3.5. Gamma-ray Upper Limits for Other High Magnetic Field Pulsars

To calculate an upper limit on pulsed flux, we simulated a point source at the position of the pulsar using the Science Tool *gtobssim* and the *P6_V3_DIFFUSE* IRFs. We used the actual pointing history of the spacecraft to accurately account for the changes in rocking profile during the mission. Such profile changes affect the exposure a given source receives and can appreciably alter sensitivity. The time intervals of the simulations are limited to the range of validity of the timing solution for each pulsar, an integration time of about 73, 82, and 87 weeks for the pulsars J1718−3718, J1734−3333, and

J1846−0258. Since there is no detection, pulsed or otherwise, of these three pulsars, we adopted a spectral shape for the simulated source typical of the shape observed for other LAT pulsars, namely a power law with exponential cut-off (see Eq. 1), with $\Gamma = 1.5$, $E_c = 3\,\mathrm{GeV}$, and $\beta = 1$. We note that higher values of E_c and lower values of Γ — i.e., sources with a greater fraction of their emission at higher energies, where the LAT has superior angular resolution and the Galactic diffuse emission is less intense — are easier to detect with both pulsed and unpulsed methods. In addition to the candidate pulsar, we simulated events from the Galactic (*gll_iem_v02*) and isotropic (*isotropic_iem_v02*) diffuse backgrounds.

Next we modeled the pulsar's light curve as a single Gaussian peak and assigned to each simulated "pulsar" photon a phase drawn at random from this light curve. To the diffuse background photons we assigned a phase drawn at random from a uniform distribution. To calculate the significance of pulsation, we selected photons from a 5×5 grid of circular apertures constructed such that all included photons had a reconstructed position within δ deg of the point source and a reconstructed energy above a threshold E_{th}, with δ linearly spaced between $0°.5$ and $1°.0$, and E_{th} uniformly spaced in logarithmic energy between $100\,\mathrm{MeV}$ and $1\,\mathrm{GeV}$. For each photon set, we calculated the H-test statistic (de Jager & Büsching 2010), and the pulsed significance was determined as the chance probability of the maximum observed test statistic multiplied by a "trials factor" of 25. This combination of pulsation test statistic and grid search yields good sensitivity to pulsations for a source of unknown spectrum and unknown light curve in an arbitrary background.

To determine the upper limit on pulsed emission, we simulated an ensemble of 20 sources at a series of integral fluxes, and for each ensemble we determined the distribution of pulsation significances via the above method. The upper limit was then simply the flux at which 68% of the sources had a pulsed significance above a given threshold, here taken to be 5σ, or a chance probability less than 5.8×10^{-7}. We note there is an approximately linear relationship between the flux threshold derived and the significance threshold, so the results reported here can be scaled to less stringent detection criteria. Finally, we perform this exercise for a series of light curves by varying the width of the gaussian peak. The results, shown in Figure 5, encompass both the sharp peaks typical of γ-ray pulsar emission and broader sinusoidal peaks.

Finally, we verified the accuracy of the technique by performing a similar exercise with actual LAT data in place of the simulated background. The resulting limits agree closely with those derived from simulation, indicating the impact of neglecting the contributions of other point sources to the background is unimportant in deriving the pulsed detection thresholds.

3.6. Gamma-ray Luminosity and Efficiency

As argued by Harding & Muslimov (2002), pulsars that produce electron-positron pairs through curvature radiation have their primary acceleration limited by the effect of screening of the electric field. This property implies that the high-energy luminosity

$$L_\gamma = 4\pi f_\Omega G_{100} d^2 \;\mathrm{erg\,s}^{-1} \qquad (2)$$
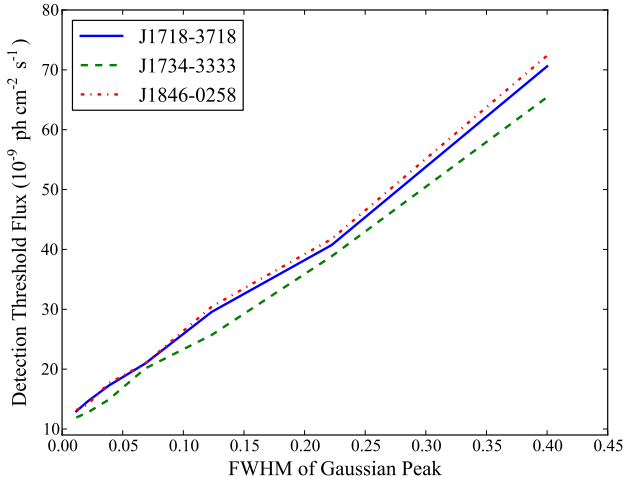
FIG. 5.— The detection threshold for pulsed emission assuming a 100% pulsed fraction from three pulsars as a function of peak width. The width is characterized by the FWHM of single gaussian peak of the assumed light curve, and the flux reported is that for which 68% of the simulated sources have a pulsed significance (calculated according to the method described in the main text) greater than 5σ. The integral flux reported is for photon energies above 100 MeV.

is proportional to $\dot{E}^{1/2}$, and that γ-ray efficiency $\eta_\gamma = L_\gamma/\dot{E}$ increases with decreasing spin-down power. In Eq. 2, d is the pulsar distance, f_Ω is the geometrical correction factor depending on the inclination and viewing angles α, ζ (see §3.4), and G_{100} is the energy flux measured above 0.1 GeV. Figure 6 shows for the studied pulsars, as well as the normal γ-ray pulsars reported in the first *Fermi*-LAT Pulsar Catalog (Abdo et al. 2010d) and Theureau et al. (2011), the L_γ as a function of $\dot{E}$. The reported values are based on the pulsar distances discussed in this paper, and under the assumption that $f_\Omega = 1$ in order to compare the results with the pulsar catalog.

For PSR J1119−6127, summing the distance and G_{100} uncertainties in quadrature yields $L_\gamma = (54 \pm 6 \pm 8) \times 10^{34} f_\Omega$ erg s^{-1}. This places the pulsar between the heuristic constant voltage line $L_\gamma^h = 10^{33} \times (\dot{E}/10^{33})^{1/2}$ erg s^{-1} represented by the dot-dashed line and the line for 100% conversion efficiency ($L_\gamma = \dot{E}$). This value confirms that in the range 10^{35} erg s$^{-1} < \dot{E} < 10^{36.5}$ erg s^{-1}, L_γ seems flat. For the emission models discussed in §3.4, the derived flux correction factors are $f_\Omega = 1.50$ (OG) and $f_\Omega = 0.95$ (TPC), and hence the luminosity cited above may be underestimated for the OG model.

For PSR J1846−0258, we derived from the upper limit on pulsed flux a luminosity of $(26 \pm 19) \times 10^{34} f_\Omega$ erg s^{-1}, using a distance of 7.9 ± 2.8 kpc and assuming a Gaussian peak with a FWHM of 0.2. The upper limit overlaps the L_γ^h line for small distances (~ 5 kpc), which is more constraining if PSR J1846−0258 behaves as a rotation-powered pulsar. However for large distances in the direction of the far side of the Sagittarius arm, the upper limit is well above the constant line, matching the luminosity of PSR J1420−6048.

For PSRs J1718−3718 and J1734−3333, the derived upper limits on the pulsed luminosity are well above 100% efficiency, and are thus unconstraining. However, these values may be biased by the adopted distances, which are based on the DM.

4. DISCUSSION

The physics close to the surface of a neutron star with a magnetic field comparable to the quantum-critical field ($B_{\rm cr} = 4.4 \times 10^{13}$ G) requires a full QED (quantum electrodynamics) treatment (see Harding & Lai 2006, for a review), and we outline a few of the salient features here. With this strong field, the cyclotron energy ($\hbar\omega_c$) equals the rest mass of the electron and is much larger than the Coulomb energy. Particles flow primarily along field lines, and particle momentum transverse to the field lines is quantized in Landau levels. Resonant absorption and emission into/from these states is a primary feature of the radiation spectra. Most importantly, the strong field enables otherwise forbidden processes such as single photon pair creation $\gamma \rightarrow e^+e^-$ and photon splitting $\gamma \rightarrow \gamma\gamma$ to proceed, and in fact become quite probable. Intense pair creation is usually invoked as a probable seed for significant radio emission (e.g. Sturrock 1971). Yet these two processes can act to suppress the overall yield of created electron-positron pairs, in turn possibly leading to radio quiet high-B pulsars and magnetars (Baring & Harding 1998): photon splitting, because it can operate below the $\gamma \rightarrow e^+e^-$ threshold of $2m_ec^2$, and pair creation, because when $B \gtrsim 6 \times 10^{12}$ G, it generates pairs in the ground state (Baring & Harding 2001), thereby inhibiting cascading and subsequent pair creation. The precise level of reduction of the pair yield by these physical mechanisms is contingent upon a number of factors, especially the photon emission/attenuation locale, and is therefore somewhat uncertain, as discussed at length by Baring & Harding (2001). Moreover, radio emission from several high-B pulsars (Camilo et al. 2000) and magnetars (Camilo et al. 2006, 2007; Levin et al. 2010) has been detected, a direct indication that the radio signal is not totally suppressed. Perhaps it originates from a higher altitude where the magnetic field is weaker and pair suppression is limited.

For γ-ray emission originating near the surface of the neutron star, the influence of the high magnetic field appears as a super-exponential cut-off in the γ-ray spectrum if one-photon pair-creation attenuation dominates (Daugherty & Harding 1982), while a more gradual cut-off is expected if photon-splitting dominates (Harding et al. 1997). These low altitude processes cannot modify γ-ray emission originating in the outer magnetosphere. As we argue below, the similarity of the observational characteristics of PSR J1119−6127 to other "normal" γ-ray pulsars implies any connection between the high surface magnetic field and high-altitude γ-ray emission is weak. This is underpinned by the exponential character of the turnover in Figure 2. As discussed for other *Fermi* LAT pulsars, the maximum energy ϵ_{max} of the pulsations provides a lower limit to the altitude of γ-ray emission, since it must lie below the γ-B magnetic absorption threshold. Assuming a dipole field, this provides an estimate of the minimum emission altitude $r > (\epsilon_{max}B_{12}/1.76\,{\rm GeV})^{2/7}P^{-1/7}R_*$ (inverting Eq. 1 of Baring 2004), where $B_{12} = B_s/10^{12}$ G is the scaled sur-
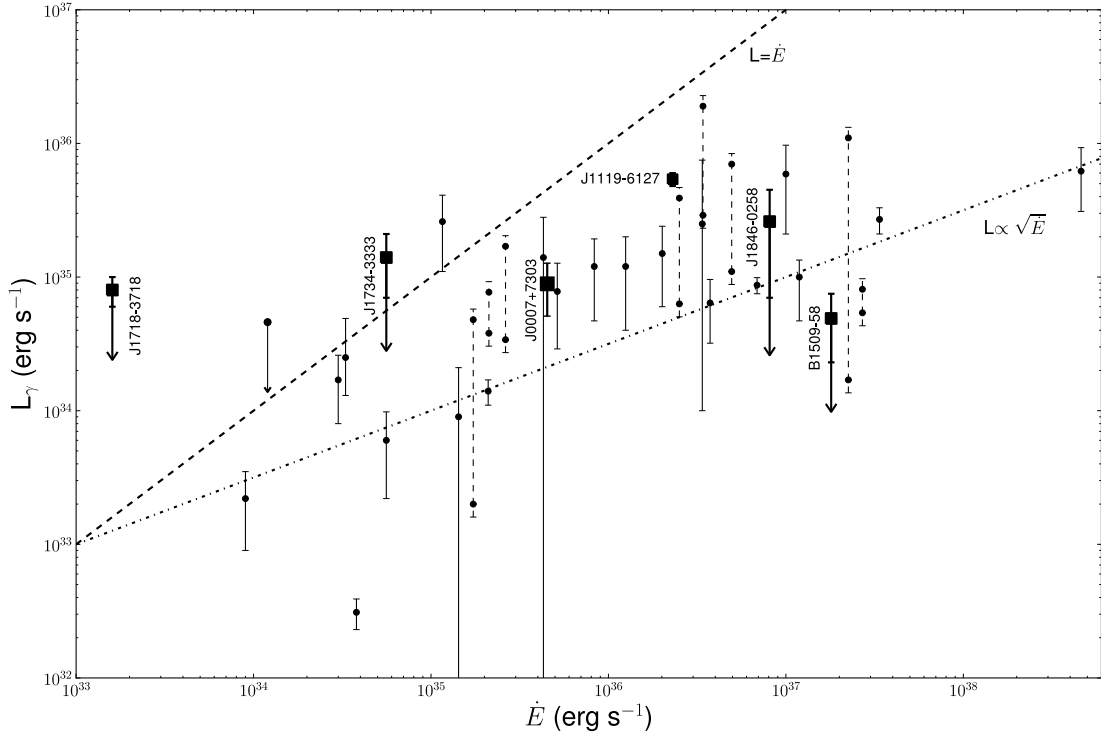
FIG. 6.— Gamma-ray luminosity above 100 MeV versus the rotational energy loss rate $\dot{E}$. Dashed line: L_γ equal to $\dot{E}$. Dot-dashed line: L_γ proportional to the square root of $\dot{E}$. Black points: radio-loud and radio-quiet/faint pulsars. The values are extracted from the first LAT pulsar catalog (Abdo et al. 2010d), with the addition of PSRs J0248+6021 and J2240+5832 (Theureau et al. 2011). Pulsars with two distance estimates have two markers connected with dashed error bars. The high-B pulsars are indicated by black squares and the values are reported in Table 1.

face magnetic field and R_* is the neutron star radius. For PSR J1119−6127 we observed pulsations up to $\epsilon_{max} \sim 4\,\text{GeV}$, which places a robust lower limit of $r \gtrsim 4.2\,R_*$, thereby precluding emission near the stellar surface.

In the following subsections, we first compare the detection of PSR J1119−6127 with the two other high-field γ-ray pulsars, namely PSR B1509−58 (Abdo et al. 2010a) and the radio-quiet pulsar J0007+7307 in CTA1 (Abdo et al. 2008). We then will discuss possible explanations for the non-detection in γ-rays of PSR J1846−0258.

4.1. *PSR J1119−6127*

The characteristics of PSR J1119−6127 determined with *Fermi* are remarkably similar to those of the majority of the *Fermi*-detected young pulsars (Abdo et al. 2010d). The delay between the radio peak and the γ-ray peak, the γ-ray pulse profile, and the GeV spectrum indicate an outer-magnetosphere geometry with a preference for the OG model as shown in the light-curve modeling (see §3.4, Fig.4). At such high altitudes, the fields are far lower than B_{cr}: observe that for PSR J1119−6127, $B_{LC} = 5.7 \times 10^3\,\text{G}$ is somewhat high, but not as extreme as that of other γ-ray pulsars. This new γ-ray detection also demonstrates that a pulsar with higher B_s than PSR B1509−58 can emit γ-rays (Abdo et al. 2010a), and clearly shows that the emission mechanism is more complex. While PSRs B1509−58 and J1119−6127 have similar ages, braking indices, and surface magnetic fields, PSR B1509−58 has a complex light curve with one of the

two γ-peaks slightly preceding the radio peak and a softer γ-ray spectrum breaking in the MeV band (Kuiper et al. 1999; Abdo et al. 2010a). Neither of these two observed features is fully explained by the high-altitude emission models. Moreover, while PSR B1509−58 shows a non-thermal component up to 10 MeV and turns over in the MeV bands, PSR J1119−6127 presents only thermal emission below 10 keV but emits GeV pulsations. Comparing PSR J1119−6127 with the CTA1 pulsar, it is interesting to note that apart from similarities in the GeV spectrum (cut-off energy at a few GeV) and soft X-ray pulsations (mainly below 2 keV, Caraveo et al. 2010), no radio pulsations for CTA1 were detected in spite of deep searches (Halpern et al. 2004). One likely explanation is that the radio beam does not sweep across our line of sight, and this suggests that the emission geometry (α, ζ) is different than in PSR J1119−6127.

4.2. *PSR J1846−0258 and other high-B pulsars*

Based on its high $\dot{E} = 8.1 \times 10^{36}\,\text{erg s}^{-1}$, hard X-ray emission (e.g. Kuiper & Hermsen 2009, $\Gamma = 1.20 \pm 0.01$, 20–250 keV), and its young age, PSR J1846−0258 seems to be a good γ-ray pulsar candidate. However, we detect no γ-ray pulsations from this object, and no source from the 1FGL catalog coincides with the pulsar position. A first explanation for the non-detection of PSR J1846−0258 can be simply a matter of its geometry. Torus modeling in the PWN implies a line of sight angle $\zeta = 62° \pm 5°$ (Ng et al. 2008). Livingstone et al. (2006) infer a magnetic inclination α about 10° using spin-down

parameters applied to the model of an oblique rotator with a current-starved outer magnetosphere (Melatos 1997). With these ζ and α values it is unlikely that low-altitude radio emission will be observed. Indeed, adopting these angles no γ-ray emission is expected from the OG, whereas from the TPC model non-pulsed (DC) or broad single-peaked pulsed emission would still be possible (Watters et al. 2009). We stress that these predictions are highly dependent on the correctness of the model by Melatos (1997).

Another possibility is that the sensitivity of the *Fermi* LAT is insufficient to detect PSR J1846−0258. The pulsar is near the Galactic plane, 30° away from the Galactic center where the diffuse γ-ray background is very strong. According to the upper limit on pulsed flux presented in §3.5 and the distance of $7.9 \pm 2.8\,\mathrm{kpc}$, the derived γ-ray efficiency is less than 0.03 ± 0.02. The Vela pulsar, which has a well-constrained distance around $300\,\mathrm{pc}$, and shows a similar spin-down power ($\dot{E} = 7 \times 10^{36}\,\mathrm{erg\,s^{-1}}$), has a γ-ray efficiency of 0.01 ± 0.002, which is just at the limit of PSR J1846−0258. In summary, the appreciable distance and high background could make the γ-ray detection of this pulsar difficult.

Finally, we cannot rule out that the γ-ray spectrum of PSR J1846−0258 resembles the very soft γ-ray spectrum of PSR B1509−58. In X-rays, PSR J1846−0258 mimics PSR B1509−58 in many ways. They both emit pulsed non-thermal hard-X-ray emission up to ~ 250 keV (~ 10 MeV for PSR B1509−58) with broad asymmetric single-peak pulse profiles with similar hard spectral shapes ($\Gamma \sim 1.2$–1.4), and neither shows soft thermal emission below $2\,\mathrm{keV}$ (except during the 2006 outburst of PSR J1846−0258), although such a signal could be swamped by the non-thermal emission. The pulsed flux of PSR B1509−58 is $\sim 2 \times 10^{-10}$ erg cm^{-2} s^{-1} (< 250 keV), which is about an order of magnitude higher than that of PSR J1846−0258 (Marsden et al. 1997; Cusumano et al. 2001). If the spectrum of PSR J1846−0258 peaks in the MeV range as in the case of PSR B1509−58, then the sensitivity of *Fermi* would also be insufficient to measure its pulsations.

The upper limits on emission from PSRs J1718−3718 and J1734−3333—which could be quiescent magnetars for which we have not yet detected magnetic activity—are not constraining. Zhang & Jiang (2005) studied OG (Zhang et al. 2004) predictions of energetic high-B pulsars before the launch of *Fermi*. Assuming $\alpha = 55°$, they predicted all pulsars in our sample to be detectable with the *Fermi* LAT. However, they assumed a sensitivity of 2×10^{-9} ph cm^{-2} s^{-1} (> 100 MeV) for a 2-year all-sky survey, which is not realistic along the Galactic plane where the diffuse background is very high (see Fig. 9, Abdo et al. 2010d). Note that for PSR J1119−6127 the predicted γ-ray flux is an order of magnitude below our observations.

In conclusion, *Fermi* observations of high-B pulsars are as yet insufficient to determine whether these objects form a homogeneous class or have both a "normal" component and a "magnetar" component. Of the pulsars with fields above 10^{13} G, only the soft spectrum of PSR B1509−58 is anomalous, whereas the other features are compatible with emission from other, lower-field γ-ray pulsars. On the other hand, PSR J1846−0258 has shown magnetar-like behavior, but the *Fermi* non-detection is not constraining. Note that the same high-B field effects that are in place in the magnetospheres of these pulsars might also affect magnetars' emission. The non-detection of any SGR or AXP with the *Fermi*-LAT is not surprising in the context of our results. Several magnetars have rotational energies and distances comparable to the high-B pulsars we report here, but no significant γ-ray emission has been detected yet (Abdo et al. 2010c). The best hope for resolving the issue may lie with future X-ray polarization measurements (such as with *GEMS* [21] or a successor), which can probe the spin and magnetic geometry of these high-B pulsars. These measurements, together with deeper *Fermi* limits, may constrain or even exclude emission from the outer magnetosphere. If true, this would indicate that some high-B pulsars are quiet in the $> 100\,\mathrm{MeV}$ γ-ray band, and thus form a distinct class of objects that resemble magnetars in some of their characteristics. At present, it must also be emphasized that PSRs J1718−3718, J1734−3333 and PSR J1846−0258 are distant and in the general direction of the Galactic center, raising the possibility that it is difficult to isolate their signals from the diffuse γ-ray background.

5. SUMMARY

We have presented the detection of PSR J1119−6127, which has currently the highest inferred surface magnetic field of all *Fermi*-detected pulsars. The folded light curve shows a single peak which arrives with a phase delay of 0.43 ± 0.02 after the radio peak. No significant pulsations have been detected below $500\,\mathrm{MeV}$. The spectrum above $0.1\,\mathrm{GeV}$ can be described with a hard power law with an exponential cut-off ($\Gamma = 1.0 \pm 0.3^{+0.4}_{-0.2}$, $E_{\mathrm{c}} = 0.8 \pm 0.2^{+2.0}_{-0.5}\,\mathrm{GeV}$), and is similar to other normal γ-ray pulsars, except for PSR B1509−58. Fits of the pulse profile to emission models implies that the most likely emission geometry is that described by the Outer-Gap model. The best-fit parameter region (within radio-polarization boundary conditions) indicates a line of sight $\zeta = 145°$ and a magnetic inclination angle $\alpha \sim 125°$. Finally, from all these observations, the pulsar appears similar to a normal young γ-ray pulsar with no evidence for a magnetar-like behavior.

For the other three high-B pulsars in the sample we have presented pulsed-emission upper limits as a function of pulse width. For PSRs J1718−3718 and J1734−3333 limits are not low enough to constrain the emission geometry due to the low spin-down power and the distance, while for the excellent candidate PSR J1846−0258, the non-detection may suggest that the pulsar has a peculiar geometry, a low energy cut-off in its spectrum, or the *Fermi* LAT sensitivity is insufficient due to the distance and the high diffuse background.

---

[21] http://heasarc.nasa.gov/docs/gems/

TABLE 1
Measured and derived parameters for high-Magnetic-Field Rotation-Powered Pulsars

Parameters	J1718−3718	J1734−3333	J1846−0258	J1119−6127	B1509−58[d]	J0007+7303[e]
Period, P (s)	3.378	1.169	0.325	0.408	0.151	0.316
Period derivative, $\dot{P}$ (10^{-12} s s^{-1})	1.61	2.28	7.08	4.02	1.54	0.36
Surface magnetic field, B_s (10^{13} G)	7.4	5.2	4.9	4.1	1.5	1.1
Magnetic field at light cylinder, B_{LC} (10^3 G)	0.018	0.307	13.2	5.67	42.2	3.21
Age, τ_c (kyr)	33.5	8.1	0.7	1.6	1.6	13.9
$\dot{E}$ (10^{34} erg s^{-1})	0.16	5.6	810	230	1800	45
Distance, d (kpc)	4.5 ± 0.5	$6.1^{+1.6}_{-1.0}$	7.9 ± 2.8	8.4 ± 0.4	5.2 ± 1.4	1.4 ± 0.3
Braking index, n	...	1.0 ± 0.3^f	2.65 ± 0.01^g	2.684 ± 0.002^h	2.839 ± 0.003^i	...
Timing data span (months)	17	19	20	29	...	...
Radio-γ peak offset, δ	...	...	...	0.43 ± 0.02	0.96 ± 0.01	...
γ-ray peak multiplicity	...	...	...	1	2	2
γ-ray peak separation, Δ	...	...	...	one peak	0.37 ± 0.02	0.23 ± 0.01
Photon flux, $^a F_{100}$ (10^{-8} cm^{-2}s^{-1})	< 3.8	< 3.6	< 4.0	$9.3 \pm 1.2 \pm 2.0$	...	30.7 ± 1.3
Energy flux, $^a G_{100}$ (10^{-11} erg cm^{-2}s^{-1})	< 3.3	< 3.1	< 3.5	$6.4 \pm 0.5 \pm 1.0$	< 1.5	38.2 ± 1.3
Energy cut-off, E_c (GeV)	...	...	...	$0.8 \pm 0.2^{+2.0}_{-0.5}$	...	4.6 ± 0.4
Spectral Index, Γ	...	...	...	$1.0 \pm 0.3^{+0.4}_{-0.2}$	...	1.38 ± 0.05
Luminosity, $^b L_\gamma$ (10^{34} erg s^{-1})	$< 8 \pm 2$	$< 14 \pm 7$	$< 26 \pm 19$	$54 \pm 6 \pm 8$	$< 4.9 \pm 2.6$	8.9 ± 3.8
Efficiency, $^b \eta$	$< 50 \pm 10$	$< 2.5 \pm 1.0$	$< 0.03 \pm 0.02$	$0.23 \pm 0.03 \pm 0.04$	$< 0.003 \pm 0.002$	0.20 ± 0.08

References. — [d]Abdo et al. (2010a); [e]Abdo et al. (2010d); [f]Espinoza et al. (2010); [g]Livingstone et al. (2006); [h]Weltevrede et al. (2010a); [i]Livingstone et al. (2005)

Note. — The upper limits on pulsed flux for PSRs J1718−3718, J1734−3333, and J1846−0258 assume a Gaussian peak with a FWHM of 0.2 for the γ-ray profile, and an exponentially cut-off power-law spectrum (see Eq. 1) with $\Gamma = 1.5$, $E_c = 3$ GeV, and $\beta = 1$. The upper limit for PSR B1509−58 is extracted from Abdo et al. (2010a) using the LAT 0.1-0.3 GeV upper limit in Fig. 3.

[a] $E > 0.1$ GeV
[b] f_Ω is assumed to be 1 which can result in an efficiency > 1.
[c] The errors on the upper limits are dominated by the distance uncertainties.

REFERENCES

Abdo, A. A., et al. 2008, Science, 322, 1218, (Fermi-LAT Collaboration - CTA 1)

—. 2009, Astroparticle Physics, 32, 193, (Fermi-LAT Collaboration - Calibration)

—. 2010a, ApJ, 714, 927, (Fermi-LAT Collaboration - PSR B1509-58)

—. 2010b, ApJS, 188, 405, (Fermi-LAT Collaboration - 1FGL Catalog)

—. 2010c, ApJ, 725, L73, (Fermi-LAT Collaboration - Magnetars)

—. 2010d, ApJS, 187, 460, (Fermi-LAT Collaboration - PSR Catalog)

Ackermann, M., et al. 2011, ApJ, 726, 35, (Fermi-LAT Collaboration - PWN)

Archibald, A. M., Kaspi, V. M., Livingstone, M. A., & McLaughlin, M. A. 2008, ApJ, 688, 550

Atwood, W. B., et al. 2009, ApJ, 697, 1071

Bai, X., & Spitkovsky, A. 2010, ApJ, 715, 1282

Baring, M. G. 2004, Advances in Space Research, 33, 552

Baring, M. G., & Harding, A. K. 1998, ApJ, 507, L55

—. 2001, ApJ, 547, 929

Blaskiewicz, M., Cordes, J. M., & Wasserman, I. 1991, ApJ, 370, 643

Camilo, F., Kaspi, V. M., Lyne, A. G., et al. 2000, ApJ, 541, 367

Camilo, F., Ransom, S. M., et al. 2007, ApJ, 666, L93

Camilo, F., et al. 2006, Nature, 442, 892

Caraveo, P. A., De Luca, A., et al. 2010, arXiv:1010.4167

Caswell, J. L., McClure-Griffiths, N. M., & Cheung, M. C. M. 2004, MNRAS, 352, 1405

Cheng, K. S., Ho, C., & Ruderman, M. 1986a, ApJ, 300, 500

—. 1986b, ApJ, 300, 522

Cordes, J. M., & Lazio, T. J. W. 2002, arXiv:astro-ph/0207156

Crawford, F., Gaensler, B. M., et al. 2001, ApJ, 554, 152

Crawford, F., & Keim, N. C. 2003, ApJ, 590, 1020

Cusumano, G., Mineo, T., Massaro, E., et al. 2001, A&A, 375, 397

Daugherty, J. K., & Harding, A. K. 1982, ApJ, 252, 337

de Jager, O. C., & Büsching, I. 2010, arXiv:1005.4867

Djannati-Ataï, A., et al. 2009, (HESS J1119−614) http://cxc.harvard.edu/cdo/snr09/pres/DjannatiAtai_Arache_v2.pdf

Dyks, J., & Harding, A. K. 2004, ApJ, 614, 869

Dyks, J., & Rudak, B. 2003, ApJ, 598, 1201

Espinoza, C. M., Lyne, A. G., Kramer, M., Manchester, R. N., & Kaspi, V. M. 2010, Nature, submitted

Everett, J. E., & Weisberg, J. M. 2001, ApJ, 553, 341

Gavriil, F. P., Gonzalez, M. E., Gotthelf, E. V., Kaspi, V. M., Livingstone, M. A., & Woods, P. M. 2008, Science, 319, 1802

Gonzalez, M., & Safi-Harb, S. 2003, ApJ, 591, L143

Gonzalez, M. E., Kaspi, V. M., Camilo, F., Gaensler, B. M., & Pivovaroff, M. J. 2005, ApJ, 630, 489

Gotthelf, E. V., Vasisht, G., Boylan-Kolchin, M., & Torii, K. 2000, ApJ, 542, L37

Halpern, J. P., Gotthelf, E. V., Camilo, F., Helfand, D. J., & Ransom, S. M. 2004, ApJ, 612, 398

Harding, A. K., Baring, M. G., et al. 1997, ApJ, 476, 246

Harding, A. K., & Lai, D. 2006, Reports on Progress in Physics, 69, 2631

Harding, A. K., & Muslimov, A. G. 2002, ApJ, 568, 862

Hobbs, G., Lyne, A. G., Kramer, M., Martin, C. E., & Jordan, C. 2004, MNRAS, 353, 1311

Hobbs, G. B., Edwards, R. T., & Manchester, R. N. 2006, MNRAS, 369, 655

Jahoda, K., Swank, J. H., et al. 1996, in SPIE Conference Series, ed. O. H. Siegmund & M. A. Gummin, Vol. 2808, 59–70

Kaspi, V. M., & McLaughlin, M. A. 2005, ApJ, 618, L41

Kuiper, L., & Hermsen, W. 2009, A&A, 501, 1031

Kuiper, L., Hermsen, W., et al. 1999, A&A, 351, 119

Leahy, D. A., & Tian, W. W. 2008, A&A, 480, L25

Levin, L., et al. 2010, ApJ, 721, L33

Livingstone, M. A., Kaspi, V. M., & Gavriil, F. P. 2010, ApJ, 710, 1710

Livingstone, M. A., Kaspi, V. M., Gavriil, F. P., & Manchester, R. N. 2005, ApJ, 619, 1046

Livingstone, M. A., Kaspi, V. M., Gotthelf, E. V., & Kuiper, L. 2006, ApJ, 647, 1286

Manchester, R. N., & Hobbs, G. 2010, MNRAS, in prep.

Marsden, D., et al. 1997, ApJ, 491, L39

Mattox, J. R., et al. 1996, ApJ, 461, 396

McLaughlin, M. A., et al. 2006, Nature, 439, 817

Melatos, A. 1997, MNRAS, 288, 1049

Mereghetti, S. 2008, A&A Rev., 15, 225

Morris, D. J., et al. 2002, MNRAS, 335, 275

Muslimov, A. G., & Harding, A. K. 2004, ApJ, 606, 1143

Ng, C., Slane, P. O., et al. 2008, ApJ, 686, 508

Olausen, S. A., Kaspi, V. M., Lyne, A. G., & Kramer, M. 2010, arXiv:1007.1196

Pivovaroff, M. J., Kaspi, V. M., Camilo, F., Gaensler, B. M., & Crawford, F. 2001, ApJ, 554, 161

Ray, P. S., Kerr, M., Parent, D., et al. 2011, ApJS, 194, 17

Rea, N., et al. 2010, Science, 330, 944

Romani, R. W. 1996, ApJ, 470, 469

Romani, R. W., & Watters, K. P. 2010, ApJ, 714, 810

Safi-Harb, S., & Kumar, H. S. 2008, ApJ, 684, 532

Smith, D. A., et al. 2008, A&A, 492, 923

Spruit, H. C. 2008, in AIP Conference Series, Vol. 983, 40 Years of Pulsars: Millisecond Pulsars, Magnetars and More, 391–398

Sturrock, P. A. 1971, ApJ, 164, 529

Su, Y., Chen, Y., Yang, J., et al. 2009, ApJ, 694, 376

Theureau, G., Parent, D., Cognard, I., et al. 2011, A&A, 525, A94+

Thompson, D. J. 2008, in AIP Conference Series, Vol. 983, 40 Years of Pulsars: Millisecond Pulsars, Magnetars and More, ed. C. Bassa, Z. Wang, A. Cumming, & V. M. Kaspi, 56–63

Watters, K. P., Romani, R. W., Weltevrede, P., & Johnston, S. 2009, ApJ, 695, 1289

Weltevrede, P., Johnston, S., & Espinoza, C. M. 2010a, MNRAS

Weltevrede, P., et al. 2010b, PASA, 27, 64

Woods, P. M., & Thompson, C. 2006, in Cambridge Astrophysics Series, Vol. 39, Compact stellar X-ray sources, ed. W. Lewin & M. van der Klis, 547

Zhang, L., Cheng, K. S., Jiang, Z. J., & Leung, P. 2004, ApJ, 604, 317

Zhang, L., & Jiang, Z. J. 2005, ApJ, 632, 523

Zhu, W. W., Kaspi, V. M., McLaughlin, M. A., Pavlov, G. G., Ng, C.-Y., Manchester, R. N., Gaensler, B. M., & Woods, P. M. 2011, ApJ, 734, 44